Semiconductor Science and Technology

PAPER

Electrochemically synthesized $CuInSe_2$ thin films from non-aqueous electrolyte for solar cell applications

To cite this article: Priyanka U Londhe *et al* 2016 *Semicond. Sci. Technol.* **31** 125009

IOP Publishing Semiconductor Science and Technology
Semicond. Sci. Technol. 31 (2016) 125009 (11pp) doi:10.1088/0268-1242/31/12/125009

Electrochemically synthesized $CuInSe_2$ thin films from non-aqueous electrolyte for solar cell applications

Priyanka U Londhe, Ashwini B Rohom, Manorama G Lakhe, Ganesh R Bhand and Nandu B Chaure

Department of Physics, Savitribai Phule Pune University, Pune-411007, India

E-mail: n.chaure@physics.unipune.ac.in

Received 21 May 2016, revised 6 August 2016
Accepted for publication 15 September 2016
Published 10 November 2016

Abstract

Highly polycrystalline $CuInSe_2$ (CIS) thin films have been electrodeposited from non-aqueous ethylene glycol (EG) solvent on fluorine-doped tin-oxide-coated glass substrates at 130 °C. The co-deposition potential for Cu, In and Se was optimized by using cyclic voltammetry. CIS layers have been electrodeposited from −1.1 V to −1.5 V versus the Ag/AgCl reference electrode. The effect of selenization on structural, morphological, optical and compositional properties has been studied extensively. Highly crystalline CIS thin films are electrodeposited for all reported growth potentials without post-annealing treatment. The Raman spectra of stoichiometric CIS thin films showed a dominant A1 mode with features receptive to the crystalline quality of the layers. Noticeable changes in the surface morphology and composition of films deposited at different deposition potential were observed. All CIS layers were void free, compact, uniform, and well adherent to the substrates with particle size ~1–3 μm. Both as-deposited and selenized samples were Cu-rich, however, the composition of selenium remained closer to the ideal value, 50%. A typical solar cell prepared at −1.3 V measured $V_{OC} = 0.316$ V, $J_{SC} = 26$ mA, $FF = 49$, and $\eta = 4.2$, under illuminated conditions at 100 mW cm^{-2}.

Keywords: $CuInSe_2$, selenization, non-aqueous bath, electrodeposition, thin-film solar cells

(Some figures may appear in colour only in the online journal)

1. Introduction

The increasing demand for energy and limited fuel resources is forcing researchers to find alternative sources of renewable energy. Amongst the various types of renewable energy, solar energy is considered as one of the prime potential contenders for generating electrical energy to gratify the growing demand. Thus, the development of photovoltaic (PV) technologies has arisen due to the growing interest in the production of electrical power from renewable sources. Solar energy conversion is part of a long-term strategy to guarantee a stable and sufficient supply of electrical power in the future. Thin-film solar cells are thriving and projected to grow appreciably, because of the low production costs, and the fact that they offer a wide variety of choices in terms of device design and fabrication. Among the various thin-film absorbers, the potential low-cost materials of current interest are amorphous Si (a-Si-H), CdTe, $CuInTe_2$ and $CuInSe_2$/$CuInGaSSe_2$, CZTS, etc [1–7]. Although (a-Si-H) solar cells have many advantages, the cell efficiency is comparatively low (~10%) [8] and there are unresolved issues related to degradation. The maximum reported efficiency of the CdTe cell is ~21.5% [9]. However, the toxicity of Cd makes them less environmentally friendly. Chalcopyrite semiconductors are considered a good alternative to the silicon-based materials and most capable absorber materials in thin-film solar cells. Among thin-film PV devices, solar cells using copper-indium-diselenide as an absorber show the highest efficiency. Non-vacuum, low-cost methods are desirable to prepare the absorber layers with controlled stoichiometry for solar cell development. So improving the performance and reducing the production costs of CIS/CIGS solar cells are current fields of

study. Solution-based techniques are low-cost methods for the deposition of absorber CIS/CIGS thin films.

The electrochemical route is one of the techniques that has been widely investigated. This method involves either a) one-step electrodeposition [10]; or b) sequential electrodeposition of the elemental layer followed by post-heat treatment to produce the required ternary or quaternary compound [11]. Single–step cathodic electrodeposition of ternary or quaternary compound in aqueous electrolyte is complicated due to the wide difference in the redox potentials of metal ions. The reduction of In ions in aqueous electrolyte requires a high negative overpotential with respect to the redox-coupled potential of Cu and Se ions. This results in less indium content in the precursor layer. Some studies on the electrochemical mechanism of indium deposition from an acidic bath showed the early formation of Cu_xSe_y on the working electrode, with consequent incorporation of indium in the precursor layer. Therefore, the Cu_xSe_y phase may act as the nuclei site for the incorporation of indium in the deposit, which may lead to poor crystallinity of the films with secondary phases along with CIS compound of various structures [12]. Post-heat treatments then become a necessary part of the film preparation. To overcome this problem, research is still being conducted on different aspects of the electrochemical parameters on the morphology, crystallinity and composition, such as the chemistry of the electrolyte, deposition potential, pH, precursor concentration, complexing agents, etc. Currently, the potentiostatic deposition of CIS/CIGS layers in chloride [13] or sulfate [10]-based aqueous bath at room temperature is the routine method with some improvements. In spite of the many advantages of electrodeposition, poor crystallinity and stoichiometry (undesired binary phases) due to In and Ga deposition rates are limited by H^+ reduction. This causes composition inhomogeneity and pinholes, which directly affect the efficiency of the solar cell [14–16]. Due to the liberation of hydrogen during electrolysis, narrow electrochemical windows, low thermal stability, and evaporation of the solution in aqueous electrolyte, scientists have sought new non-aqueous solutions to electrodeposit materials. Some ionic liquids and alcohols are used for the electrodeposition of CIGS thin films. Peter *et al* [17] first reported the electrodeposition of Cu–In, Cu–In–Se and Cu–In–Ga–Se precursor thin films in ionic liquid (Reline) to form CIS and CIGS. Harati *et* al also used the same electrolyte for the deposition of stoichiometric CIGS without post-heat treatment. Dimethyl sulfoxide (DMSO) was used as the solvent for the growth of CIGS by Bhattacharya *et al* [18]. The electrodeposition of CIS from a non-aqueous bath has been reported by Dharmadasa *et al* [19] onto FTO-coated glass substrate. The present studies investigate the possibility of the deposition of highly crystalline CIS layer from ethylene glycol (EG), which has high viscosity, a high boiling point (197 °C), a wide electrochemical window, high thermal stability and good solubility of a large number of organic and inorganic compounds.

2. Materials and methods

2.1. Sample preparation

One-step electrodeposition in a non-aqueous medium (ethylene glycol) was employed for the deposition of CIS layers. The CIS films were deposited potentiostatically onto FTO-coated glass substrates at 130 °C using Biologic potentiostat/galvanostat model SP150.

To understand the electrochemical mechanism of the co-deposition of Cu, In and Se in EG, initially the electrochemistry of individual Cu, In and Se was studied using cyclic voltammetry (CV) measurements. The solution matrix contains copper (II) chloride ($CuCl_2$), indium chloride ($InCl_3$) and selenium tetrachloride ($SeCl_4$). LiCl was used as a supporting chemical compound to control the ionic conductivity of the electrolyte. A standard three-electrode geometry with Ag/AgCl as reference, FTO as working and graphite as counter electrode were used. CV measurements and the deposition of CIS films were performed without agitation at 130 °C. CIS films deposited for a wide potential range −1.1 to −1.5 V versus Ag/AgCl were optimized from CV measurements. Chronoamperometry is studied for different potentials. Immediately after the deposition, the layers were ultrasonically cleaned in boiled distilled water to remove the residue and/or the traces of EG. Subsequently, the layers were dried in a stream of N_2 gas. CIS layers were selenized in a homemade tubular selenization chamber to improve the crystallinity, homogeneity and particle size. The films were placed in the quartz holder at a distance ∼20 mm above the selenium ingots of ∼1 gm. A two-step annealing process was employed to selenize the samples at rotary vacuum $\sim 5 \times 10^{-2}$ Torr. Initially, the chamber was heated at ∼200 °C for 15 min to melt the Se ingots. Subsequently, the temperature was raised to 400 °C (40° min^{-1}) and maintained for 20 min.

2.2. Characterization techniques

Various characterization techniques are used to study the properties of as-deposited and selenized CIS thin films deposited at various potentials. The surface topography was examined using a JEOL JSM-6360A scanning electron microscopy (SEM) at accelerating voltage 20 kV and probe current 1 nA. The EDAX attachment available with the SEM instrument was employed to determine the compositional analysis. The thickness of the layers was measured by a Filmetrics F10 thin-film analyzer. The phases and crystal structures of the CIS films deposited at various potentials were characterized by x-ray diffractometer, Model Bruker D8, with CuKα radiation of wavelength 1.5405 Å. The optical properties were studied by using a JASCO UV–vis-NIR spectrophotometer. Raman scattering experiments were carried out using a Invia Renishow micro-Raman spectrophotometer with the help of a 785 nm emission line. The final solar cell devices were measured upon illumination with 100 mW cm^{-2}.

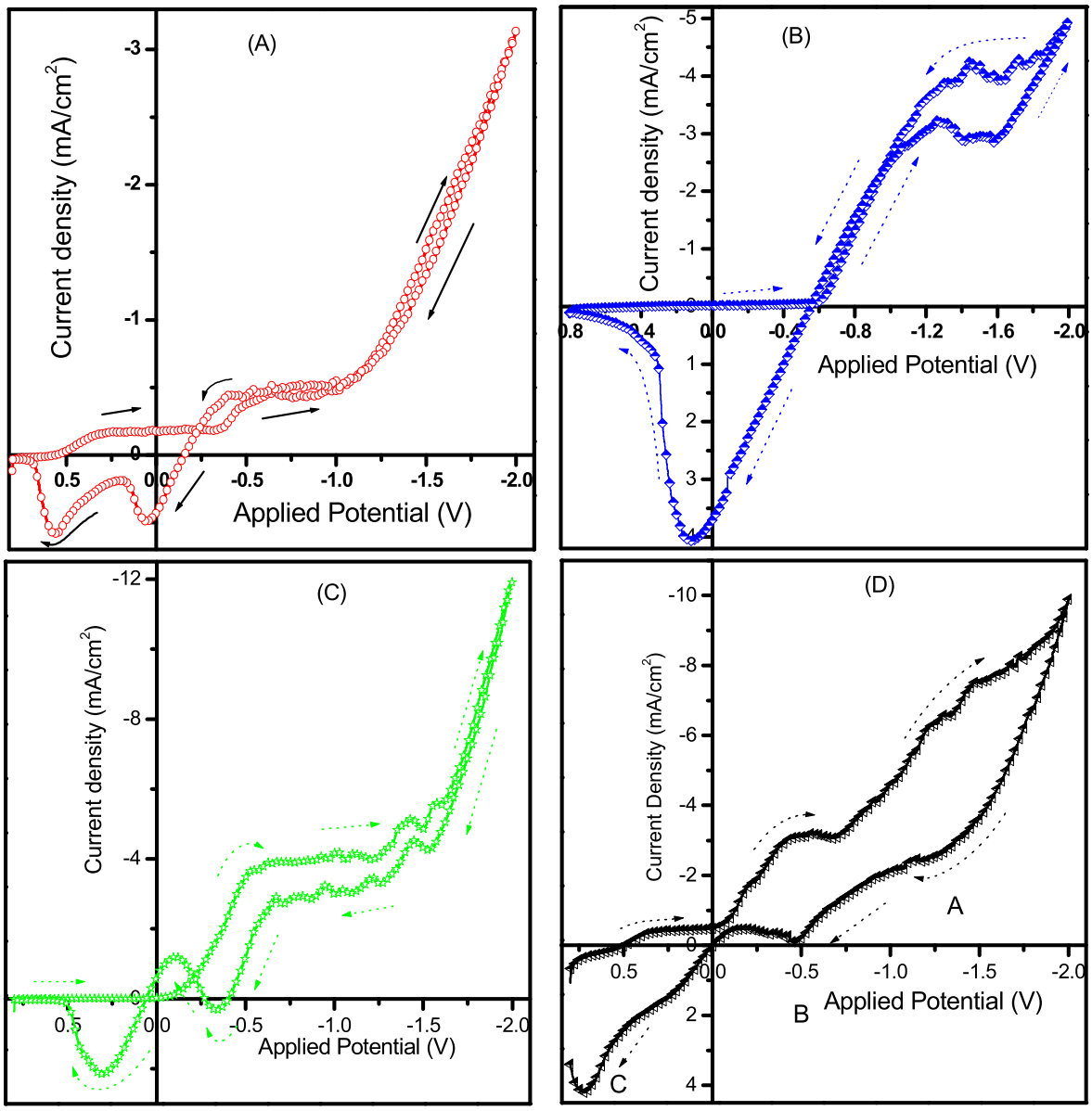

Figure 1. A typical CV recorded in EG as an electrolyte consisting of ionic species $CuCl_3$ (A), $InCl_3$ (B) and $SeCl_4$ (C) and combined $CuCl_3$, $InCl_3$ and $SeCl_4$ (D) with a scan rate of 10 mV s^{-1} at a temperature of 130 °C using the Ag/AgCl reference electrode on FTO-coated glass substrate. LiCl was used as a supporting chemical compound to control the ionic conductivity of the bath.

3. Results and discussion

3.1. Cyclic voltammetry study

To study the electrochemical behavior, cyclic voltammograms (CV) for the unitary Cu, In, Se and ternary Cu-In-Se system was recorded. Figure 1 shows CV for the unitary $CuCl_2$ (A), $InCl_3$ (B) and $SeCl_4$ (C) solution and ternary Cu-In-Se solution (D) in EG at 130 °C without agitation on the FTO substrate. All the above CV's were recorded in the presence of LiCl, which acts as an additive to improve the conductivity of the bath. The CVs were recorded in the range +0.8 to −2.0 V versus the Ag/AgCl reference electrode with a scan rate of 10 mV s^{-1}. During the forward scan, two cathodic peaks are attributed to the unitary Cu system. The first peak that exhibited ~ +0.35 V could be associated to the reduction of Cu^{2+} to Cu (equation (1)) and second peak observed ~ −0.48 V can be assigned to the reduction of Cu^{2+} to Cu^{+} and later Cu^{+} to Cu by charge-transfer reactions 2 and 3, respectively. This deviation in the reduction potentials from standard values could be due to the change in open circuit potentials measured prior to beginning the CV measurements.

In the anodic scan, two peaks are observed, ~0.1 and ~0.6 V that correspond to the oxidation of Cu^{+} to Cu^{2+} and Cu to Cu^{2+}, respectively.

$$Cu^{2+} + 2e^{-} \rightarrow Cu \quad E_o = +0.34 \text{ V versus SCE} \qquad (1)$$

$$Cu^{2+} + e^{-} \rightarrow Cu^{+} \quad E_o = +0.16 \text{ V versus SCE} \qquad (2)$$

$$Cu^{+} + e^{-} \rightarrow Cu \quad E_o = +0.52 \text{ V versus SCE} \qquad (3)$$

CV recorded for the unitary $InCl_3$ in EG solution at 130 °C is

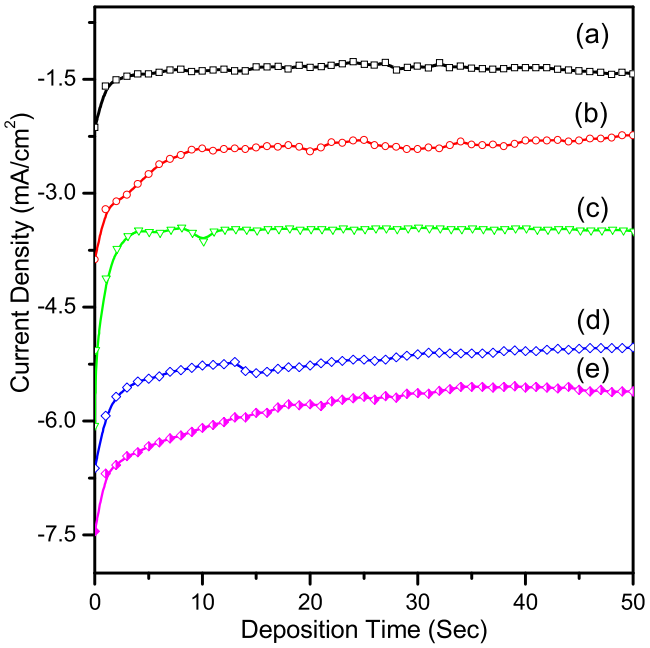

Figure 2. Chronoamperometry study of CIS films electrodeposited at −1.1 V (a), −1.2 V (b), −1.3 V (c), −1.4 V (d), and −1.5 V (e).

depicted in figure 1(B). Initially, the cathodic current remained unchanged up to −0.6 V. The rise in the cathodic current beyond −0.65 V is thought to be due to the reduction of In^{3+} to In according to the following charge-transfer reaction (4).

$$In^{3+} + 3e^- \rightarrow In \quad E_o = -0.34 \text{ V versus SCE} \qquad (4)$$

Figure 1(C) represents the CV recorded for unitary $SeCl_4$ in EG solution at 130 °C in the presence of LiCl. A very small cathodic current was measured up to −0.08 V in the cathodic scan. A clear plateau region that was observed from −0.50 to −1.50 V could correspond to the deposition of selenium according to the following charge-transfer reactions.

$$Se^{4+} + 4e^- \rightarrow Se \quad E_o = +0.84 \text{ V versus SCE} \qquad (5)$$

and/or

$$Se^{4+} + 6e^- \rightarrow Se^{2-} \quad E_o = +0.048 \text{ V versus SCE} \qquad (6)$$

Figure 1(D) exhibits the CV for a ternary Cu-In-Se system in EG solution at 130 °C. The reduction peaks observed in CV around +0.34 and −0.45 V are similar to those described in the preceding section for the reduction of Cu and Se. Further linear rise in the cathodic current after −0.7 V with increasing the cathodic potential may be due to the deposition of In along with Cu and Se. Beyond −1.1 V, the observed cathodic current increase may be due to the co-deposition of Cu, In and Se. We have not observed any bubbling from the cathode for higher cathodic potentials, which confirms the absence of hydrogen evolution. The peaks observed during the anodic scan marked as 'A', 'B', and 'C' are the stripping of In, Cu and Se, respectively. As a clear plateau region was not observed in the CV measurements, the CIS layers were

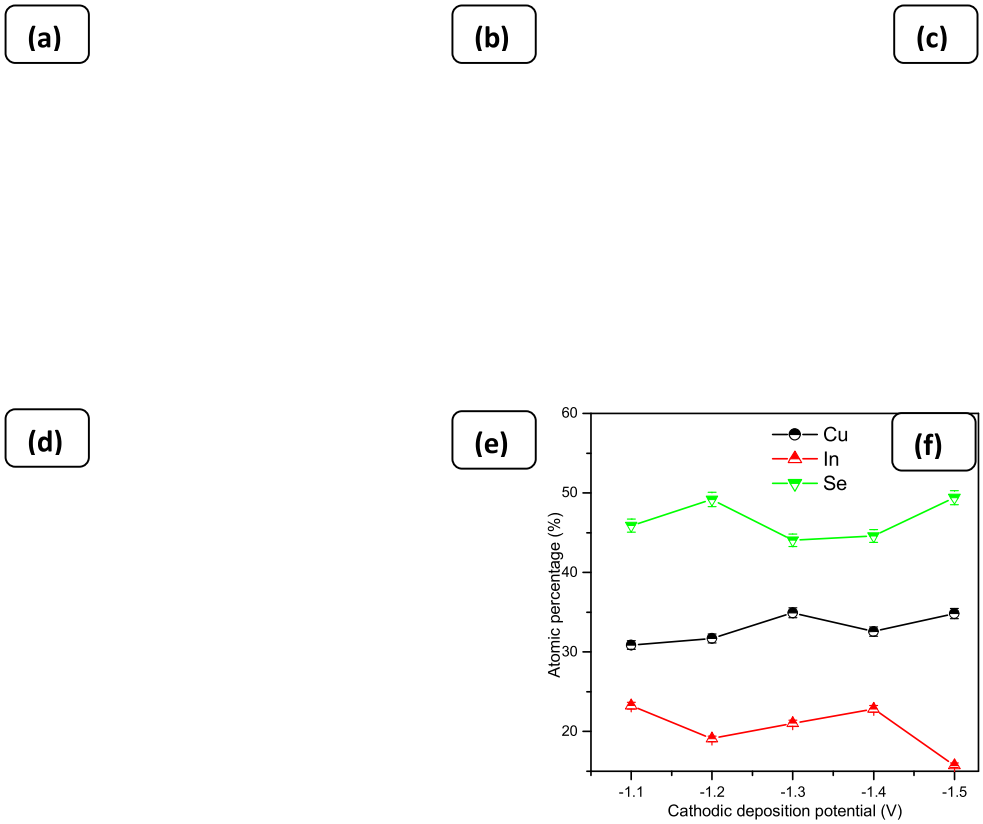

Figure 3. (**A**). SEM images of as-prepared CIS films electrodeposited at −1.1 V (a), −1.2 V (b), −1.3 V (c), −1.4 V (d), and −1.5 V (e) and (f) elemental atomic percentage concentration obtained by EDAX. (**B**). SEM images of selenized CIS films electrodeposited at −1.1 V (a), −1.2 V (b), −1.3 V (c), −1.4 V (d), and −1.5 V (e) and (f) elemental atomic percentage concentration obtained by EDAX.

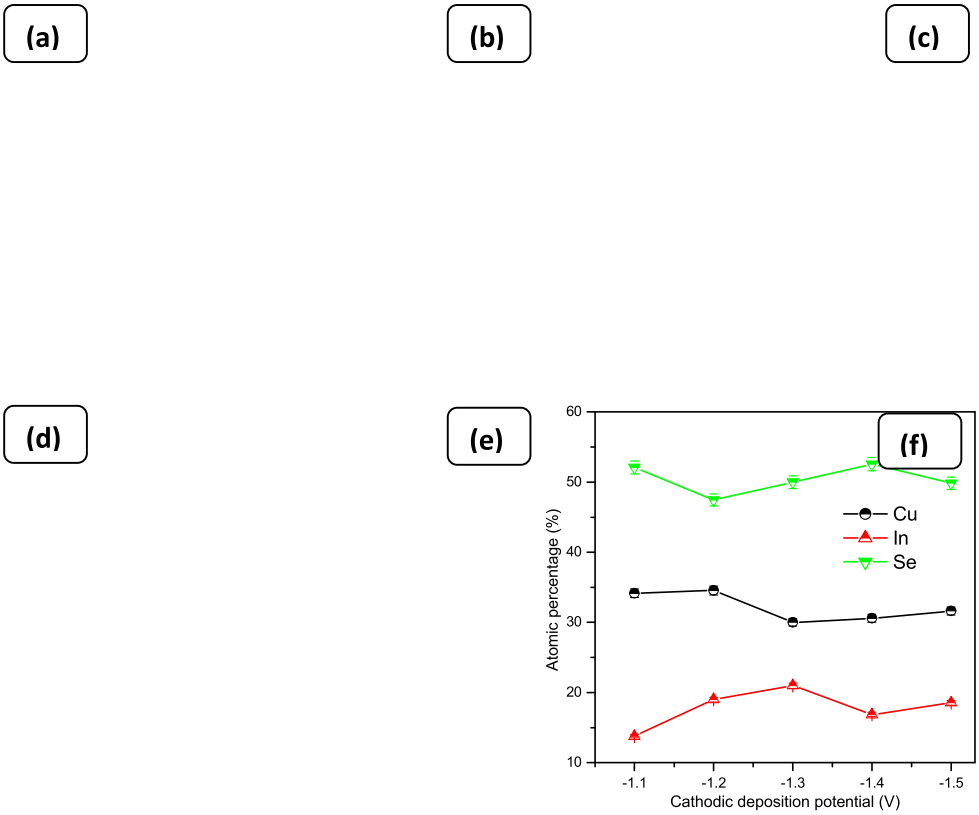

Figure 3B. (Continued.)

Table 1. A summary of thicknesses measured for as-deposited and selenized CIS layers deposited at various growth potentials.

	Thickness (μm)	
Deposition Potential (V)	As-deposited	Selenized
−1.1	2.42 ± 0.05	2.35 ± 0.05
−1.2	2.59 ± 0.05	2.45 ± 0.05
−1.3	2.71 ± 0.05	2.61 ± 0.05
−1.4	2.87 ± 0.05	2.72 ± 0.05
−1.5	3.20 ± 0.05	2.93 ± 0.05

electrodeposited at different potentials from −1.1 to −1.5 V versus Ag/AgCl onto FTO substrate.

3.2. Chronoamperometry measurements

Figure 2 shows chronoamperometric plots for CIS films electrodeposited at −1.1 V (a), −1.2 V (b), −1.3 V (c), −1.4 V (d), and −1.5 V (e). The cathodic current that decreased sharply within the first couple of seconds corresponds to the instantaneous nucleation process. The current density that was found to have increased with increasing the deposition potentials is indicative of the diffusion-controlled mechanism dominating over the charge-transfer-controlled process.

3.3. Morphological and compositional studies

Figure 3(A)(a)–(e) shows SEM topographical images of as-deposited CIS films prepared at different deposition potentials i.e. −1.1 to −1.5 V with the respective plot of chemical composition (f). The films deposited at lower potentials (−1.1 and −1.2 V) show uniform globular surface morphology of grain size ranging from ∼0.5–1.0 μm without pinholes, figure 3(A)(a) and (b). The film deposited at -1.3 V (figure 3(A) (c)) shows mixed spherical and belt-like morphology. The randomly oriented diffused rods of size ∼1–1.5 μm are formed for the films deposited at −1.4 V as shown in figure 3(A) (d), whereas the film deposited at −1.5 V showed long grain-like structure (figure 3(A) (e)) of sizes over a micron. The surface morphology was extensively altered with deposition potentials. In the electrodeposition technique, the bath temperature, viscosity of the solvent, chemical concentrations, distance between the electrodes, geometry of the electrodes, etc, are responsible for the adhesion, chemical composition, morphology, structure and conductivity of the layer. The limiting current density was found have increased from ∼3.70 to 6.40 mA cm^{-2} upon increasing the cathodic growth potential from −1.3 to −1.5 V. The nucleation and growth in the thin film is associated to limiting current density and can be explained by the

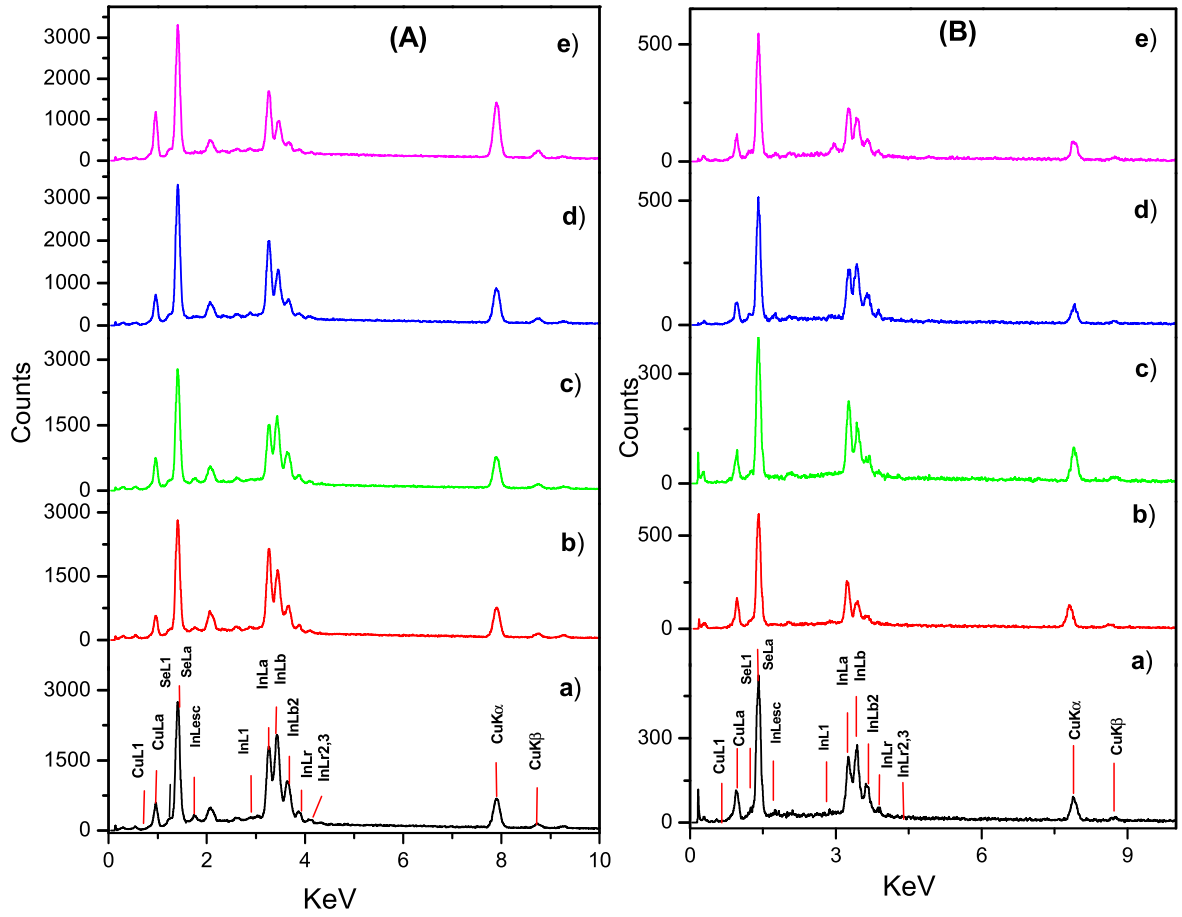

Figure 4. EDAX spectra for as-deposited (A) and selenized (B) CIS thin films electrodeposited at −1.1 V (a), −1.2 V (b), −1.3 V (c), −1.4 V (d), and −1.5 V (e).

following equation [20],

$$J(t)_{\text{lim}} = nFc\frac{D}{\delta_N} \tag{7}$$

where, $J(t)_{\text{lim}}$ is the limiting current density, t is the time, n is electrons per molecule oxidized or reduced, F is Faraday's constant, c is the bulk concentration, D_0 is the diffusion coefficient of the deposited ions, and δ_N is the diffusion-layer thickness.

Here, the electrodeposition process was performed in the unstirred electrolyte. Therefore, the diffusion layer is only dependent on the limiting current density. Increases in the limiting current density (cathodic growth potential) decrease the diffusion-layer thickness. The limiting current density determines the distribution of depositing nuclei and the morphology of the deposit. At lower current density (thicker diffusion layer) the deposition becomes charge-transfer controlled and the growth of nuclei is expected to be spherical shape. However, for higher current density (thinner diffusion layer) the growth of nuclei is in dendritic form and the deposition is diffusion controlled. Similar results of changing morphology for lithium deposition at different current densities in ionic liquids as electrolyte are observed by Hikaru *et al* [21]. Furthermore, we have measured the thickness of the as-deposited and selenized layers grown at various growth potentials and they are tabulated in table 1. The thickness of the as-deposited samples was measured between 2.42 and 3.20 μm, which is increased systematically with increasing the cathodic growth potential due to higher current density. The over-growth of the particle is expected at higher current density. The thickness measured for all selenized samples is less than the as-grown layers, probably due to the re-crystallization of the sample. In the re-crystallization process, the evaporation of Se and/or In_2Se may be responsible for reducing the thickness of the sample. The compositional analyses of the as-prepared and selenized CIS layers grown at various growth potentials obtained by EDAX are represented in figures 4(A) and (B), respectively.

Atomic composition of Cu, In and Se in all as-deposited films as a function of the deposition potential is plotted in figure 3(A) (f). The atomic percentage of copper was found to have increased with increasing the cathodic deposition potential, while the content of selenium remained at nearly ~50% for all as-deposited samples deposited at various potentials. All films were annealed in the selenium ambient at

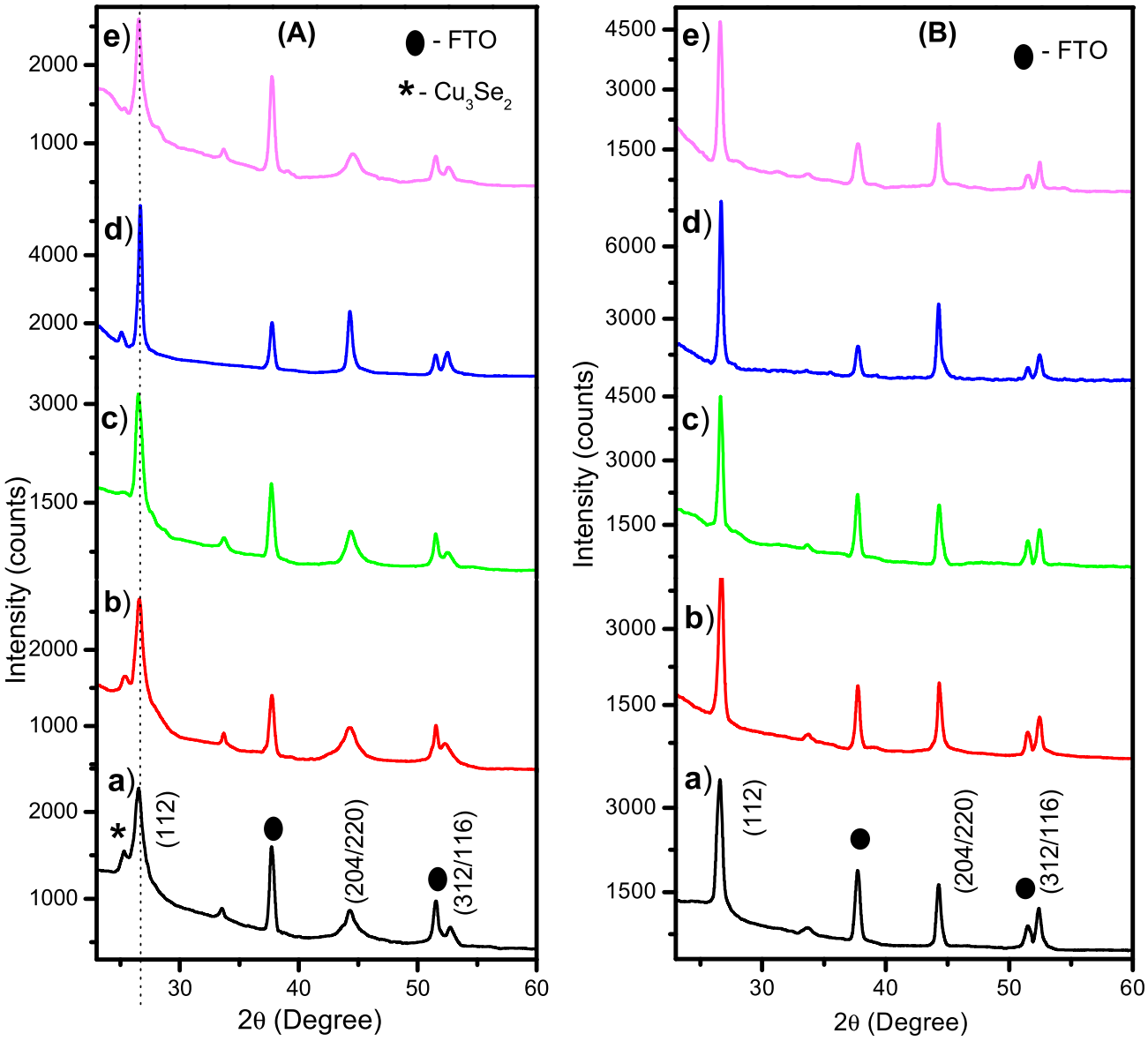

Figure 5. (**A**). X-ray diffractogram of as-prepared CIS thin films electrodeposited at −1.1 V (a), −1.2 V (b), −1.3 V (c), −1.4 V (d), and −1.5 V (e). (**B**). X-ray diffractogram of selenized CIS thin films electrodeposited at −1.1 V (a), −1.2 V (b), −1.3 V (c), −1.4 V (d), and −1.5 V (e).

400 °C for 20 min The SEM images of the selenized CIS thin films deposited for various potentials are shown in figure 3(B) (a)–(e) with corresponding compositional analysis plot (f). Densely compact surface morphology is observed for all films upon selenization. Figure 3(B) (a) shows mixed surface morphology, little micron-sized flex placed in between non-uniformly distributed spherical grains upon selenization, whereas a highly crystalline homogeneous compact layer formed for the films deposited at −1.2 V to −1.5 V (figure 3(B) (b)–(e)), which is the requirement for high-efficiency solar cells. The formation of a homogeneous layer after selenization could be due to the re-crystallization of the material. After selenization, the atomic percentage concentration of Cu was found to have been reduced and nearly stoichiometric CIS thin films were obtained at −1.4 V growth potential.

3.4. Structural study

X-ray diffraction (XRD) patterns of as-deposited and selenized CIS layers deposited at various potentials from EG at 130 °C on FTO-coated glass substrate are shown in figures 5(A) and (B), respectively. CIS thin films deposited at all growth potentials show a high degree of crystallinity with preferential (112) orientation. The XRD pattern of all as-deposited film exhibits three prominent reflections (112), (204/220) and (312)/(116) of chalcopyrite crystal structure. A broadening at the base of the first and second

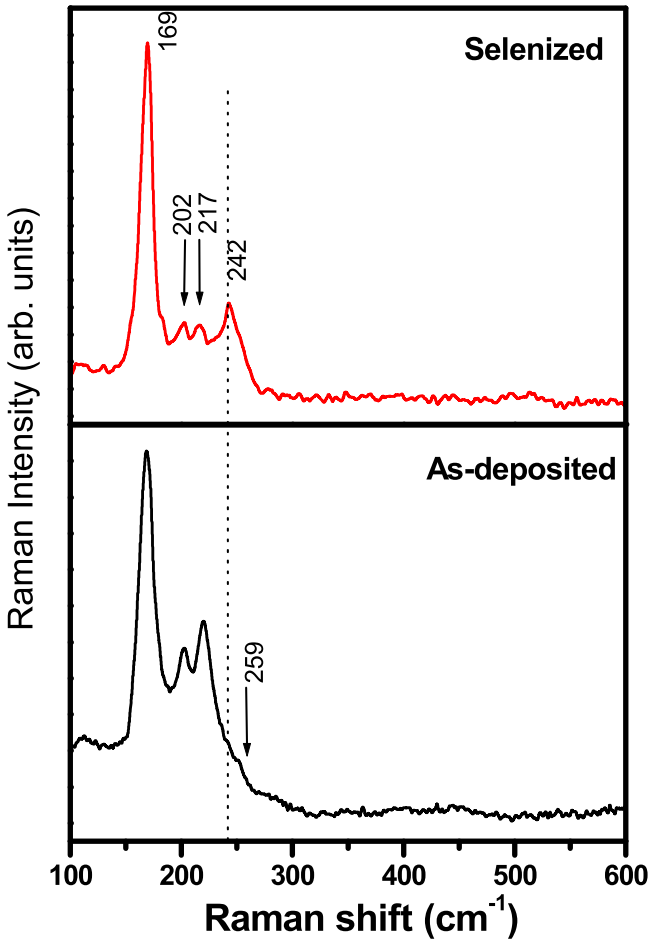

Figure 6. Raman spectra for the as-deposited and selenized CIS layer deposited at −1.3 V on FTO-coated glass substrate.

peak observed for the as-deposited sample is due to the presence of secondary phases of Cu_2Se_3 [marked as (*)]. The reflections corresponding to FTO are represented as a solid circle (•). The full width at half maximum (FWHM) calculated for the (112) peak was found to be 0.76°, 0.62°, 0.50°, 0.28° and 0.38° for the as-deposited and 0.40°, 0.35°, 0.29°, 0.24° and 0.28° for the selenized sample grown at −1.1 V, −1.2 V, −1.3 V, −1.4 V and −1.5 V, respectively. The XRD pattern of the selenized films reveals a prominent (112) preferred orientation without secondary phases and the crystallinity of all samples was found to have improved. The FWHM was decreased substantially after heat treatment. The as-prepared CIS thin films deposited from the non-aqueous bath at higher potential shows higher crystallinity than that of the annealed CIS layers deposited from the aqueous bath [22]. Therefore, the electrodeposition of CIS in the non-aqueous bath may be useful for the development of the solar cell onto flexible substrates without heat treatment or selenization.

Raman analysis, shown in figure 6, performed on the as-prepared and selenized CIS sample deposited at −1.3 V confirms the formation of the CIS layer. The most intense peak attributed at 169 cm^{-1} in both samples corresponds to the characteristics of A1 mode of the chalcopyrite CIS phase. A1 mode represents the vibration of the Se in the x–y plane with the cations at rest. Other peaks exhibited at 202 and 217 cm^{-1} are associated to the contribution of E and B2 modes of the CIS phase, respectively [23]. A small shoulder attributed at 259 cm^{-1} to the as-deposited sample is related to the Cu-Se binary phase [24]. Upon selenization, the peak corresponding to A1 mode becomes sharp, which is directly related to the improvement in the crystallinity [25]. The elemental Se peak observed at 242 cm^{-1} upon selenization could be due to the condensation of Se vapors during the natural process of cooling [26, 27]. Similar results were observed in the other selenized samples prepared at various growth potentials. Note that the selenized samples were etched in NaCN and Br-methanol solution to remove the traces of elemental Se and Se-related compounds prior to metal contact.

3.5. Optical study

Figure 7 depict the plots of $(\alpha h\upsilon)^2$ versus the energy $(h\upsilon)$ of the as-deposited and selenized CIS films electrodeposited for various growth potentials. The direct band gap (E_g) of the CIS thin films can be obtained from the intercept of the straight line on the x-axis in above graph. Band gap values for as-deposited CIS samples are found to be in the range of 1.12–1.26 eV (±0.05), whereas upon selenization the values of the band gap were close to 1.10–1.15 eV (±0.05). The higher band-gap values estimated for the as-deposited sample could be due to the presence of secondary phases. After selenization, the estimated band-gap values are in good agreement with the literature values [28, 29]. This could be due to the re-crystallization of thin films along with the homogeneous phase formation. The estimated band-gap values from the optical absorption spectra are summarized in table 2.

3.6. Optoelectronic properties

A superstrate configuration FTO/CdS/CIS/Au was completed by depositing the CdS layer using chemical bath deposition [30], CIS, absorber layer by electrodeposition at −1.3 V and Au, using thermal evaporation. The CdS/CIS layer was selenized and etched in Br-Methanol and NaCN solution prior to evaporating the Au metal contact. The final solar cell device was measured in the dark and in illuminated conditions at room temperature, as shown in figure 8. The values of the ideality factor, ideality factor $n = 1.48$, and barrier height $\Phi_B = 0.55$ eV, were calculated from the dark characteristics. A typical solar cell measured $V_{OC} = 0.316$ V, $J_{SC} = 26$ mA, $FF = 49$, and $\eta = 4.2$, under illuminated conditions of input power intensity 100 mW cm^{-2}.

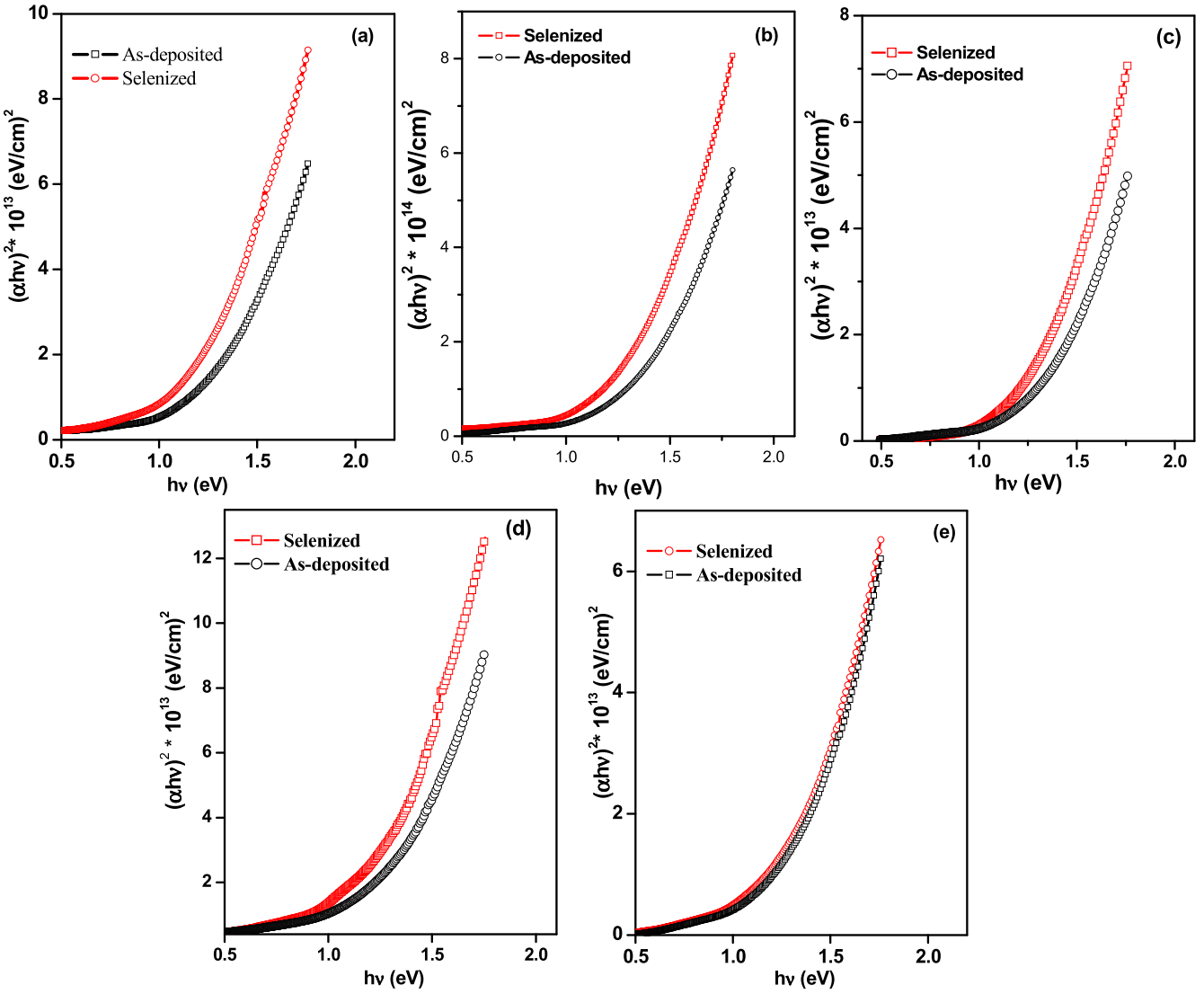

Figure 7. Optical absorption spectra recoded for the as-deposited and selenized (a)–(e) CIS thin films deposited on FTO at −1.1 V, −1.2 V, −1.3 V, −1.4 V and −1.5 V, respectively.

Table 2. A summary of band gap calculated for $CuInSe_2$ thin films deposited on FTO at various deposition potentials.

	Band gap (eV)	
Deposition Potential (V)	As-deposited	Annealed
−1.1	1.22	1.15
−1.2	1.25	1.12
−1.3	1.26	1.14
−1.4	1.23	1.11
−1.5	1.12	1.10

4. Conclusion

Systematic CV measurements were performed on the CIS system in non-aqueous electrolyte to optimize the growth potential. A wide potential window, −1.1 to −1.5 V verses the Ag/AgCl reference electrode was observed from CV measurements. XRD results revealed that the as-prepared films deposited for all potentials are highly crystalline with chalcopyrite structure, which is promising for the preparation of solar cells on flexible plastic substrate. Raman measurements confirmed the formation of the pure phase of chalcopyrite CIS. Nearly stoichiometric and highly crystalline films were obtained after selenization. Different morphology observed for the films deposited at higher potential could be due to a dominating diffusion-controlled mechanism. Higher working temperature is favorable to deposit the larger particles suitable for solar cell applications. The optical band-gap values were found to be in the range of 1.10–1.15 eV upon selenization. The values of ideality factor n = 1.48, and barrier height Φ_B = 0.55 eV, were calculated from the dark characteristics. A typical solar cell measured V_{OC} = 0.316 V, J_{SC} = 26 mA,

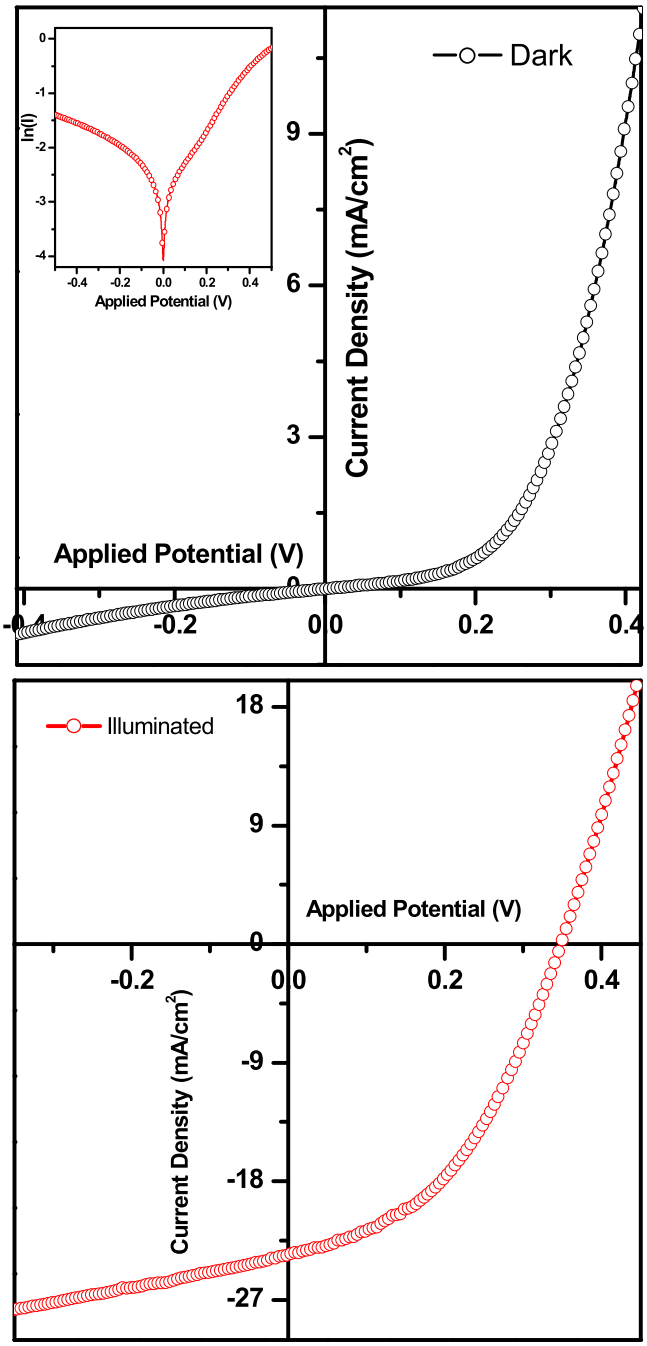

Figure 8. Dark and illuminated *J–V* curves of a FTO/CdS/CIS heterostructure solar cell device. The CIS layer was electrodeposited at −1.3 V.

FF = 49, and η = 4.2 under illuminated conditions of input power intensity 100 mW cm^{-2}.

Acknowledgments

The authors would like to thank the Defence Research and Development Organization (DRDO), New Delhi, India (ERIP/ER/10003866/M/01/1388) for providing the financial support through a major research grant.

References

[1] Chen Y H, Lin C C, Liu Y T, Lu H W and Liu J C 2016 Hydrogen dilution on an undoped silicon oxide layer and Its application to amorphous silicon thin-film solar cells *Mater. Sci. Semic. Proc.* **41** 312–6

[2] Li W, Li Y, Du G, Chen N, Liu S, Wang S, Huang H, Lu C and Niu X 2016 Enhanced electrical and optical properties of boron-doped ZnO films grown by low pressure chemical vapor deposition for amorphous silicon solar cells *Ceram. Int.* **42** 1361–5

[3] Dharmadasa I M, McLean A B, Pattersont M H and Williams R H 1987 Schottky barriers and interface reactions on chemically etched n-CdTe single crystals *Semicond. Sci. Technol.* **2** 404–12

[4] Kephart J M, Geisthardt R M and Sampath W S 2015 Optimization of CdTe thin-film solar cell efficiency using a sputtered, oxygenated CdS window layer *Prog. Photovolt. Res. Appl.* **23** 1484–92

[5] Lakhe M G, Mahapatra S K and Chaure N B 2015 Development of $CuInTe_2$ thin film solar cells by electrochemical route with low temperature (80 °C) heat treatment procedure *Mater. Sci. Eng.* B **204** 20–6

[6] Green M A, Emery K, Hishikawa Y, Warta W and Dunlop E D 2015 Solar cell efficiency tables (Version 45) *Prog. Photovolt., Res. Appl.* **23** 1–9

[7] Ingrid R, Miguel A C, Brian E, Egaas B, DeHart C, Scharf J, Perkins C L, To B and Noufi R 2008 19.9%-efficient ZnO/CdS/CuInGaSe2 solar cell with 81.2% fill factor *Prog. Photovolt., Res. Appl.* **16** 235–9

[8] Matsui T, Bidiville A, Maejima K, Sai H, Koida T, Suezaki T, Matsumoto M, Saito K, Yoshida I and Kondo M 2015 High-efficiency amorphous silicon solar cells: impact of deposition rate on metastability *Appl. Phys. Lett.* **106** 053901

[9] 'First Solar Builds the Highest Efficiency Thin Film PV Cell on Record'. (firstsolar.com)

[10] Chaure N B, Young J, Samantilleke A P and Dharmadasa I M 2004 Electrodeposition of p–i–n type $CuInSe_2$ multilayers for photovoltaic applications *Sol. Energy Mater. Sol. Cell* **81** 125–33

[11] Londhe P U, Rohom A B and Chaure N B 2014 Selenization of electrodeposited copper–indium alloy thin films for solar cell application *J. Mater. Sci., Mater. Electron.* **25** 4643–9

[12] Chassaing E, Grand P P, Ramdani O, Vigneron J and Lincot A 2010 Electrocrystallization mechanism of Cu–In–Se compounds for solar cell applications electrochemical/chemical deposition and etching *J. Electrochem. Soc.* **157** D387–95

[13] Rohom A B, Londhe P U and Chaure N B 2015 The effect of pH and selenization on the properties of $CuInSe_2$ thin films prepared by electrodeposition technique for device application *J. Solid State Electrochem.* **19** 201–10

[14] Bhattacharya R N and Fernandez A M 2003 $CuIn_{1-x}Ga_xSe_2$-based photovoltaic cells from electrodeposited precursor films *Sol. Energy Mater. Sol. Cell* **76** 331–7

[15] Cummings C, Zoppi G, Forbes I, Colombara D, Peter L M and Marken F 2012 Rocking disc electro-deposition of CuIn alloys, selenization and pinhole effect minimization in CISe solar absorber layers *Electrochim. Acta* **79** 141–7

[16] Bouroushian M, Kosanovic T, Karoussos D and Spyrellis N 2009 Electrodeposition of polycrystalline ZnTe from simple and citrate-complexed acidic aqueous solutions *Electrochim. Acta* **54** 2522–8

[17] Shivagan D D, Dale P J, Samantilleke A P and Peter L M 2007 Electrodeposition chalcopyrite films from ionic liquid electrolytes *Thin Solid Films* **515** 5899–903

[18] Bhattacharya R N, Contreras M A, Keane J, Tennant A L, Tuttle J R, Ramanathan K and Noufi R 1998 Preparation of

copper indium gallium diselenide films for solar cells *US Patent* 5 804 054

[19] Wellings J S, Samantilleke A P, Heavens S N, Warren P and Dharmadasa I M 2009 Electrodeposition of $CuInSe_2$ from EG at 150 °C *Sol. Energy Mater. Sol. Cell* **93** 1518–23

[20] Paunovic M and Schlesinger M 2006 *Fundamentals of electrochemical Deposition* 2nd edn (John Wiley & Sons. Inc.) p 95

[21] Sano H, Sakaebe H, Senoh H and Matsumoto H 2014 Effect of current density on morphology of lithium electrodeposited in ionic liquid-based electrolyte *J. Electrochem. Soc.* **161** A1236–40

[22] Donglin X, Man X, Zhuang L J and Xiujian Z 2006 Co-electrodeposition and characterization of Cu (In, Ga)Se_2 thin films *J. Mater. Sci.* **41** 1875–8

[23] Chao A, Ahn S, Yun J H, Wak J G, Ahn S K, Shin K, Song H and Yoon K H 2013 Non-vacuum processed $CuInSe_2$ thin films fabricated with a hybrid ink *Sol. Energy Mater. Sol. Cells* **109** 17–25

[24] Izquierdo-Roca V *et al* 2007 Raman microprobe characterization of electrodeposited S-rich CuIn,S,Se for photovoltaic applications: Microstructural analysis *J. Appl. Phys.* **101** 103517–8

[25] Park J H, Yang I S and Cho H Y 1994 Micro-Raman spectroscopy on polycrystalline $CulnSe_2$ formation *Appl. Phys.* A **58** 125–8

[26] Ramdani O, Guillemoles J F, Lincot D, Grand P, Chassaing E, Kerrec O and Rzepka E 2007 One-step electrodeposited $CuInSe_2$ thin films studied by Raman spectroscopy *Thin Solid Films* **515** 5909–12

[27] Motohiko shii E, Shibata K and Nozaki H 1993 Anion distributions and phase transitions in $CuS_{1-x}Se_x$ (x = 0–1) *J. Solid State Chem.* **105** 504–11

[28] Oleksak R P, Flynn B T, Schut D M and Herman G S 2014 Microwave-assisted synthesis of $CuInSe_2$ nanoparticles in low-absorbing solvents *Phys. Status Solidi* A **211** 219–25

[29] Caballero-Briones F, Palacios-Padrós A and Sanz F 2011 $CuInSe_2$ films prepared by three step electrodeposition. Deposition mechanisms, optical and photoelectrochemical studies *Electrochim. Acta* **56** 9556–67

[30] Chaure N B, Bordas S, Samantilleke A P, Chaure S N, Haigh J and Dharmadasa I M 2003 Investigation of electronic quality of chemical bath deposited cadmium sulphide layers used in thin film photovoltaic solar cells *Thin Solid Films* **437** 10–7